SHIP TECHNOLOGY RESEARCH (SCHIFFSTECHNIK)
https://doi.org/10.1080/09377255.2023.2167537

Towards a full-scale CFD guideline for simulating a ship advancing in open water

Luofeng Huang [a], Blanca Pena[b] and Giles Thomas[b]

[a]School of Water, Energy and Environment, Cranfield University, Cranfield, United Kingdom; [b]Department of Mechanical Engineering, University College London, London, United Kingdom

ABSTRACT

Computational Fluid Dynamics (CFD) simulations of a ship's operations are generally conducted at model scale, but the reduced scale changes the fluid behaviour around the ship. Whilst ideally ship simulations should be run directly at full scale, a guide has not been published to advise on the suitable setups that can provide accurate results while minimizing the computational cost. To address this, the present work explores an optimal approach for full-scale ship simulations. Extensive sensitivity studies were conducted on relevant computational setups to investigate their influences on the prediction of ship resistance, ship-generated waves as well as the boundary-layer flow of the hull. A set of CFD setups for full-scale ship simulations in open water was recommended. It was demonstrated that the ideal Y+ and Courant numbers in full scale are evidently different from those given in current model-scale CFD guidelines, indicating the necessity to establish full-scale CFD guidelines separately.

ARTICLE HISTORY
Received 24 June 2022
Accepted 8 January 2023

KEYWORDS
Ship; full-Scale; computational fluid dynamics; guideline; resistance; boundary layer; wave; sea trial

1. Introduction

Computational Fluid Dynamics (CFD) has developed into one of the essential tools for ship design, with its well-proven capabilities of predicting ship performance, including resistance, motions, manoeuvres and localized loads (el Moctar et al. 2012; Mucha 2017; Gatin et al. 2018; Huang et al. 2020). Yet most of the existing CFD work for ships is not performed at the real ship scale, as simulations are normally built at model scale to enable validation against experimental tests.

The downscaling brings about physical discrepancies though. Taking ship resistance in calm water as an example, in model experimental tests the scaling is based on a consistent Froude number (Fr), which scales the pressure component correctly but imposes errors within the friction component due to a changed Reynolds number (Re). This is because it is impossible to ensure that both Fr and Re are equal between the two scales. The mismatch in the frictional component is generally corrected using a standard extrapolation procedure of the International Towing Tank Conference (ITTC) (2008). Nevertheless, the extrapolation procedure is empirically based, thus it could provide inaccurate resistance predictions (Niklas and Pruszko 2019). Moreover, the changed Re number leads to unrealistic boundary layer and flow behaviours, which cannot be remedied by extrapolation.

By running CFD simulations directly in full scale, the scaling issues can be avoided, meaning that the fluid behaviours are replicated at the correct scale and empirically-based extrapolation procedures are not required. Detailed discussion on the scale effect between model and real ships has been documented by Terziev et al. (2022), showing the inherent errors in model-scale prediction and extrapolation is an outstanding problem for various ship design purposes. It causes incorrect reproduction of geometrical features, false prediction of flow properties such as turbulence/wave characteristics, as well as a result of disparities in force ratios acting on the model and full-scale structures (Terziev et al. 2019). Based on a thorough review, Terziev et al. (2022) demonstrated that the application of full-scale CFD should be increasingly used to overcome the scale issue for ships and its development has become a primary interest of the shipping industry (Peric 2019).

However, ship simulations in full scale are still under exploration, since the best practice for full-scale simulations differs considerably from that for model scale, which means existing guidelines for ship simulations in model scale cannot be directly used, e.g. (ITTC 2014a). This is because a full-scale computational domain will be many times larger than a model-scale domain to fit the ship, but the fluids (water and air) are the same in both scales.

CONTACT Luofeng Huang luofeng.huang@cranfield.ac.uk School of Water, Energy and Environment, Cranfield University, Cranfield, United Kingdom

This means that, whilst the domain size for full scale can be in the order of kilometres, the size of computational cells around the hull still needs to be millimetres to properly model the near-hull flow details. Consequently, the cell size around the hull needs to gradually increase towards the whole domain and sophisticated local mesh refinements are crucial, so a new meshing approach for full-scale ship simulations is required to solve the transition of cell size. This will cause other optimal setups to be different from those in model scale, such as the modelling of wall boundary layer (Peric 2019). In addition, the size of timestep will need to adapt to the full-scale meshing approach.

To provide an initial assessment on the best practice of full-scale ship simulations, Lloyd's Register (LR) (2016) organised the first-ever CFD workshop on a full-scale cargo ship, which provided a set of sea trial data as a benchmark for participants' blind simulation tests. Twenty-two sets of CFD results were received before the workshop, with various computational setups applied. The results showed generally good abilities of CFD on predicting full-scale ship performance, including resistance, power, propeller torque and vessel-generated waves. Nevertheless, the computational setups from the participants were based upon diverse strategies, and the resistance predictions differed by up to 16% from each other. Based upon analysing the inputs and outputs from the participants, the workshop concluded that further investigations are required to absorb the quintessence from each of the participants and make a set of ideal setups to be recommended for future users.

Full-scale CFD has been successfully applied to various ship hydrodynamic simulations. Niklas and Pruszko (2019) compared the resistance of a large carrier ship from full-scale CFD prediction, model test extrapolation and sea trial data. In their results, the full-scale CFD provided accurate predictions against the sea trial data for the complete examined range, while the extrapolated results from model-scale experiments were found to have large deviations in certain conditions. Haase et al. (2016, 2017) developed a full-scale CFD approach for the resistance prediction of large-scale catamarans, and then performed a comparison between full-scale CFD prediction, model test extrapolation and sea trial data. Their results showed full-scale CFD prediction generally presented much smaller deviations against the sea trial data, compared with model test extrapolation. The above outcomes suggest that full-scale CFD simulations for deriving resistance equations may be a rational alternative method to model test extrapolation.

Pena et al. (2020a, 2020b) presented detailed analyses of the flow field around an advancing cargo ship using full-scale CFD. Their results demonstrated the value of full-scale CFD for comprehensive ship design purposes, such as cavitation circumvention, flow control and hydroacoustic optimization. These analyses are not possible via model-scale CFD or experiments, since they require the flow to be kept at the correct scale. Huang et al. (2021b) simulated the slamming effect on a lifeboat by reproducing the surrounding flow at the correct scale, with computational results agreeing well with full-scale measurements. Based on sea trial data, Jasak et al. (2019) validated the performance of full-scale CFD in predicting the propeller performance of a cargo ship. They presented sophisticated local mesh refinements in their CFD model and compared it with several other mesh sets that caused inaccurate results. The work of Jasak et al. (2019) indicates an appropriate mesh setup is a key to achieving accurate full-scale CFD prediction for ships. The above types of full-scale simulation are important for structural design and hydro-vibration investigations (McVicar et al. 2018; Smith and Ventikos 2022; Huang and Li 2022). Moreover, Tezdogan et al. (2015, 2016), Nisham et al. (2021) and Terziev et al. (2021) applied full-scale CFD to analyse the behaviour of a ship in head-seas and restricted waters, which demonstrates such environmental conditions may contain significant fluid-ship interactions that need to be assessed in the real scale. Other examples of full-scale CFD for ship hydrodynamic simulations can be found as (Bhushan et al. 2009; Min and Kang 2010; Ponkratov and Zegos 2015; Liefvendahl and Fureby 2017; Bakica et al. 2020; Cheng et al. 2020)

Despite that the aforementioned examples have shown full-scale CFD can provide significant insights for ships, the existing literature has all focussed on applications rather than CFD itself. A guideline for full-scale ship CFD is still lacking, without which, relevant simulations could be conducted with setups that are unassured or even inappropriate, especially considering the scarcity of full-scale measurements for validation. In this context, the present work aims to provide an exploration for any future full-scale CFD guideline for ships. The innovation of this paper is studying full-scale ship CFD itself by systematically performing simulations with varying setups to investigate the difference and derive an ideal configuration, which has not been included in any previous work.

The work is organised as follows: first, a full-scale computational model for a cargo ship advancing in calm water was established and validated against the LR sea trials data (2016). Then, relevant computational setups (e.g. mesh density, mesh transition ratio, mesh local refinements approach, timestep size, and the orders of discretisation) were systematically varied to investigate their influences on the ship performance prediction, focussing on the prediction of ship resistance, ship-generated waves and hull boundary layer. As a result, an accurate and cost-effective approach for simulating the case was derived,

which was condensed into a set of recommendations for other CFD users.

2. Method

This section first introduces sea trials of a cargo ship that provide full-scale measurement data to be used as a benchmark for this study. Then a CFD model is built to simulate the sea trials, and the computational results are compared with the measurements to confirm the accuracy. Subsequently, a systematic research plan is proposed to investigate the sensitivities of essential CFD setups.

2.1 Benchmark ship and sea trials

A typical general cargo ship, *Regal* (Figure 1), was adopted as the ship object of this study. Sea trials of *Regal* were conducted in 2016 in the calm-water open ocean condition, during which ship power, torques and speed were recorded at three different shaft speeds (Lloyds Register 2016). The measurement uncertainties were reported to be minimal as the on-site sea condition was very calm. The main parameters of *Regal* and the sea trial conditions are given in Tables 1 and 2. Before the sea trials, the vessel was dry-docked, the hull was cleaned, and the propeller surface was polished. In this clean condition, the hull, rudder, and propeller were scanned with 3D lasers to obtain accurate geometric representations. The scanned geometries were imported into the CFD model presented in the following section.

Table 1. Main particulars of Regal.

	Symbol	Magnitude
Length between perpendiculars (m)	L_{pp}	138
Waterline beam (m)	B	23
Draught aft (m)	T	5.6
Wetted surface area (m^2)	S_w	3727
Propeller diameter (m)	D	5.2

Table 2. Sea trial conditions of Regal.

	Shaft Speed (rpm)	Speed (knots)	Re	Fr
Condition 1	71.6	9.25	7.43×10^8	0.13
Condition 2	91.1	11.60	9.32×10^8	0.16
Condition 3	106.4	13.00	1.04×10^9	0.18

(a) The vessel in sea

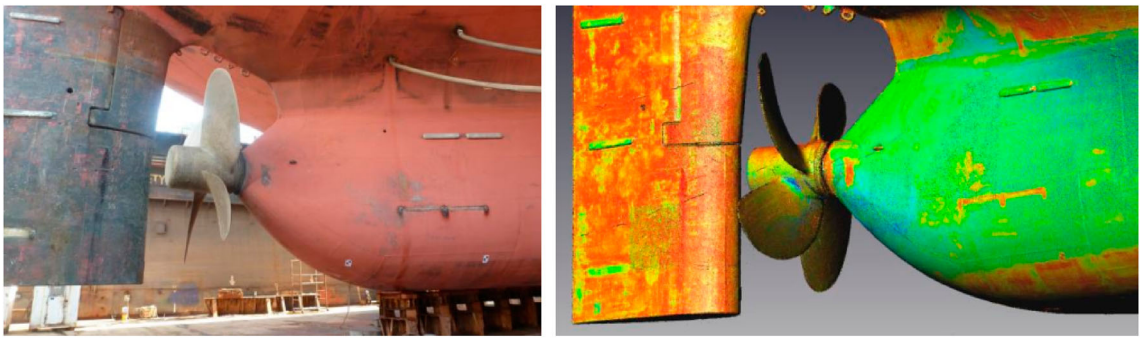

(b) Vessel in a dry-dock and 3D scan data

Figure 1. The *Regal* general cargo ship (Lloyds Register 2016). (a) The vessel in sea; (b) Vessel in a dry-dock and 3D scan data.

2.2 Computational modelling

To reproduce the sea trials, an open ocean computational domain was built based on the STAR-CCM + software. Compared with model-scale CFD approaches, the full-scale simulation does not use different governing equations or boundary conditions, while the domain size is determined based on the real ship dimensions, as shown in Figure 2. The computational domain is three-dimensional, defined by the earth-fixed Cartesian coordinate system O-*xyz*. The (*x, y*) plane is parallel to the horizon, and the *z*-axis is positive upwards. The domain size is sufficiently large to avoid the ship-generated waves being reflected from the boundaries. The lower part of the domain is filled with seawater and the remainder is filled with air. The *Regal* hull is fixed at the free surface according to the design draught whilst its trim and squat are allowed through enabling the Dynamic Fluid Body Interaction (DFBI) module. The hull surface is modelled as a no-slip wall (velocity equals zero). The water was initialized as flowing with a constant velocity (U_{water}) against the bow of the hull, and a constant velocity condition was applied to the inlet boundary to maintain a stable water flow entering the domain. Thus, a relative velocity exists between the ship and water, where U_{water} indicates the advancing speed of the ship in calm water ($U_{water} = U_{ship}$). The top, boundary and side boundaries were also set with the same constant velocity to align this relative movement. The hydrostatic pressure condition was applied to the outlet, and the velocity here meets the zero-gradient condition. Taking advantage of the symmetry of the case, only half of the ship was put into the

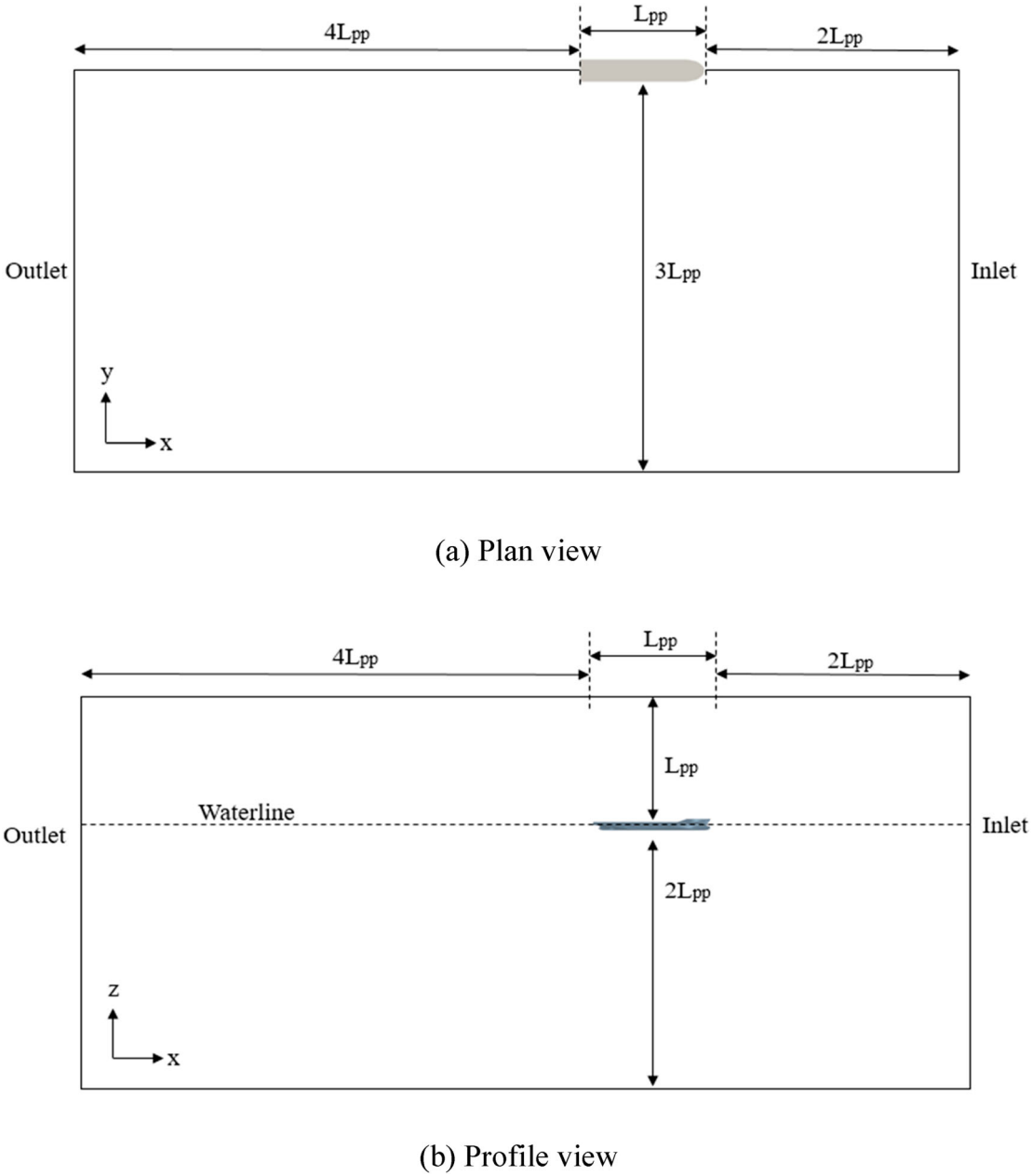

Figure 2. Computational domain with dimensions. (a) Plan view; (b) Profile view.

fluid domain, and the symmetry condition was applied on a boundary paralleling the centreplane of the ship, which can mirror the computed fluid field and save half the computational cost.

The solution of the fluid domain was obtained by solving the Reynolds-averaged Navier-Stokes (RANS) equations for an incompressible Newtonian fluid:

$$\nabla \cdot \bar{\mathbf{v}} = 0 \tag{1}$$

$$\frac{\partial(\rho\bar{\mathbf{v}})}{\partial t} + \nabla \cdot (\rho\overline{\mathbf{v}}\overline{\mathbf{v}}) = -\nabla\bar{p} + \nabla \cdot (\bar{\tau} - \rho\overline{\mathbf{v}'\mathbf{v}'}) + \rho g \tag{2}$$

where $\bar{\mathbf{v}}$ is the time-averaged velocity, $\mathbf{v}'$ is the velocity fluctuation, ρ is the fluid density, $\bar{p}$ denotes the time-averaged pressure, $\bar{\tau} = \mu[\nabla \mathrm{v} + (\nabla \mathrm{v})^{\mathrm{T}}]$ is the viscous stress term, μ is the dynamic viscosity and g is gravitational acceleration set at 9.81 m/s^2. Since the RANS equations have been adopted to account for the turbulent effects, a turbulence model needs to be applied to close the equations, for which, the Shear Stress Transport (SST) k − ω model (Menter 1993) was adopted. The logarithmic law wall function is applied to resolve the boundary layer (Peric 2019). The SST k − ω model has been demonstrated to be a robust RANS turbulence modelling strategy for ships due to its capability to model adverse pressure gradients and flow separation (Paterson et al. 2003). An adverse pressure gradient means the pressure increases in the direction of the flow, which can happen when a water flow encounters a hull, especially around the stern region (ITTC 2014a). The review of Pena and Huang (2021) shows the SST k − ω model is a comprehensive RANS scheme for ship hydrodynamic simulations in both model and full scales.

The free surface between the air and water was modelled by the Volume of Fluid (VOF) method (Hirt and Nichols 1981). The VOF method introduces a passive scalar α, denoting the fractional volume of a cell occupied by a specific phase. In this case, a value of α = 1 corresponds to a cell full of water, and a value of α = 0 indicates a cell full of air. Thus, the free surface, which is a mix of these two phases, is formed by the cells with 0 < α < 1. The elevation of the free surface along time is obtained by the advection equation of α, expressed as Equation (3). For a cell containing both air and water, its density and viscosity are determined by a linear average according to Equation (4) and Equation (5). In this study, $\rho_{\mathrm{water}} = 1010$ kg/m^3, $\mu_{\mathrm{water}} = 8.93 \times 10^{-4}$ N·s/m^2, $\rho_{\mathrm{air}} = 1.16$ kg/m^3, $\mu_{\mathrm{air}} = 1.86 \times 10^{-5}$ N·s/m^2, according to measurements in sea trials where the seawater and air temperatures were respectively 25 and 30 degrees Celsius. The governing equations of the fluid domain were discretised and solved using the Finite Volume Method (FVM) (Versteeg and Malalasekera 2007); Figure 3 shows the mesh layout of the model, in which local mesh refinements are applied around the hull, to the free surface region and where Kelvin waves are expected to occur.

$$\frac{\partial\alpha}{\partial t} + \nabla \cdot (\bar{\mathbf{v}}\alpha) = 0 \tag{3}$$

$$\rho = \alpha\rho_{water} + (1 - \alpha)\rho_{air} \tag{4}$$

$$\mu = \alpha\mu_{water} + (1 - \alpha)\mu_{air} \tag{5}$$

2.3 Verification and validation

Further verifications were conducted for the ship resistance to ensure that the numerical uncertainty is insignificant. This was also to choose a suitable mesh density to start with, minimizing the waste of computational resources. To perform the verifications, the shaft speed rpm = 106.4 was adopted, corresponding to 13 knots, which is close to the design service speed of *Regal*. The mesh of the CFD model was globally scaled into four sets of meshes, consisting of 7.5, 10.6, 15.2 and 21.1 million cells respectively, and then corresponding ship resistance results were obtained. According to Equation (6), the total resistance (R_T) is made non-dimensional into a total resistance coefficient (C_T).

$$C_T = R_T/0.5\rho_{water}S_wU_{ship}^2 \tag{6}$$

The C_T values predicted using the four sets of mesh are presented in Figure 4. It shows that C_T achieved a monotonic convergence (Celik et al. 2008): it gradually approaches a certain value and the variance is not significant when the cell number is larger than 15.2 million. Thereafter, the mesh with 15.2 million cells was selected to start further investigations. The convergence of C_T with this mesh set is presented in Figure 5. Minimal oscillation can be observed along with the convergence of the curve, where the oscillating level is less than 1% of the C_T magnitude and this can be considered reasonable during numerical calculations. This oscillating level is sufficiently small to have no impact on the present result analysis. Therefore, the simulation was not run longer for analysis and the average value was taken from the last 20 s of data. For further cases tested in Section 3, all cases will be run for 200s and taken the last 20 s data to analyse the oscillating level when the CFD inputs changed. When a large oscillation occurs for a case (> 1%), the oscillating level will be plotted as an error bar.

The timestep size for all of the four sets of mesh was controlled following a mean Courant number (Co), as

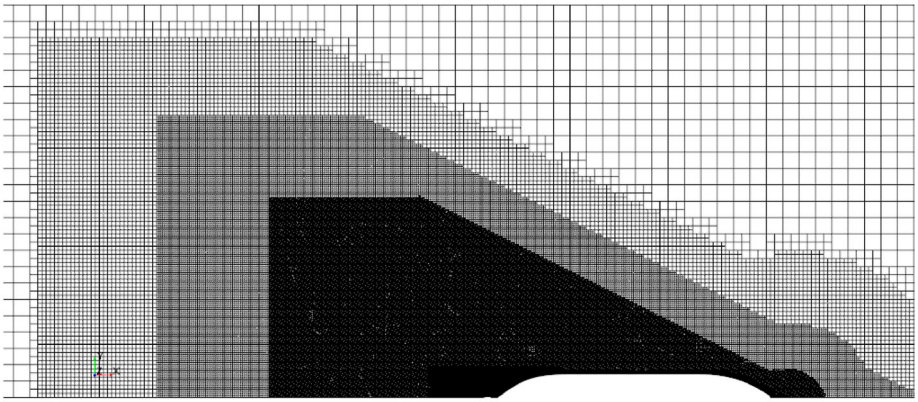

(a) Plan view

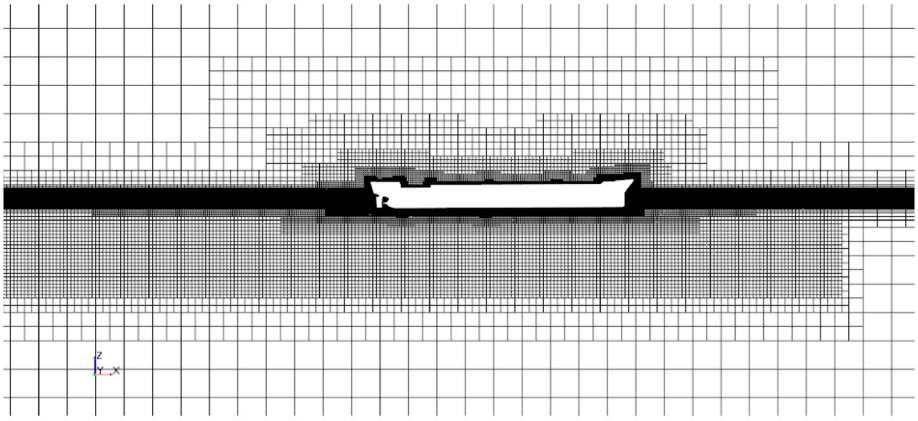

(b) Profile view

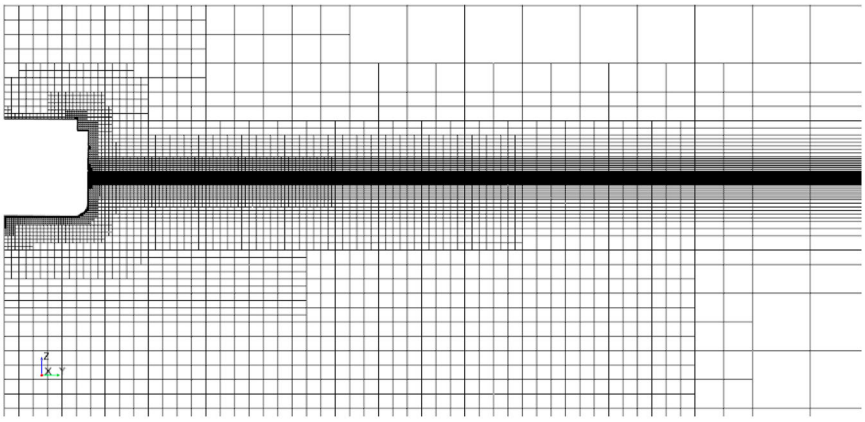

(c) Section view across midship

Figure 3. Mesh layout of the model. (a) Plan view; (b) Profile view; (c) Section view across midship.

expressed in Equation (7).

$$\mathrm{Co} = \frac{\mathrm{u}\Delta\mathrm{t}}{\Delta\mathrm{X}} \tag{7}$$

where Δt is the timestep size, $u/\Delta X$ is its normal velocity divided by the distance between the cell centre and the centre of the neighbour cell. The work started by setting $\overline{Co} \leq 10$, and this choice will be justified in Section 3.3.

Upon the verification, validation was conducted by comparing the propeller torque results from full-scale CFD with those measured during the sea trials. This validation was added as it was impossible to directly measure resistance in sea trials, thus comparison on the torque coefficient is legitimate. The comparison was performed for all three shaft speed conditions of the sea trials, as introduced in Table 2.

In the CFD simulations, a Moving Reference Frame (MRF) is applied to simulate the propeller operation,

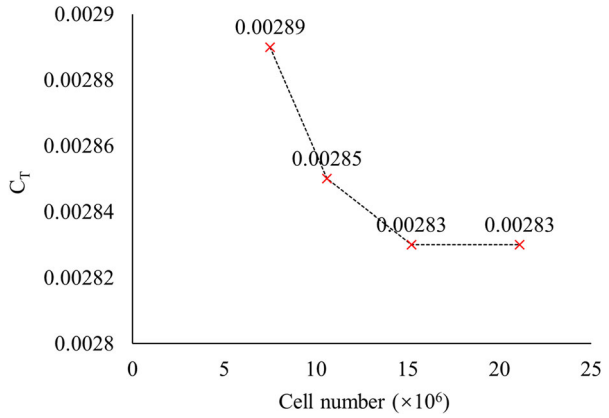

Figure 4. Total resistance coefficients obtained by CFD models of different cell numbers.

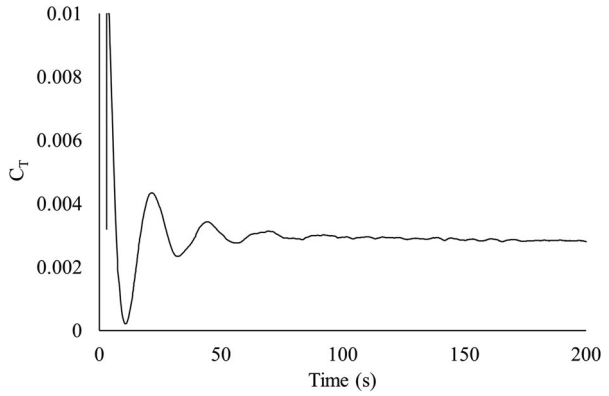

Figure 5. Time series of total resistance coefficient (cell number ≈ 15.2 million).

where the propeller rotation is modelled by using the sliding mesh technique. A refined mesh (25% of the surrounding mesh) is applied around the propeller,

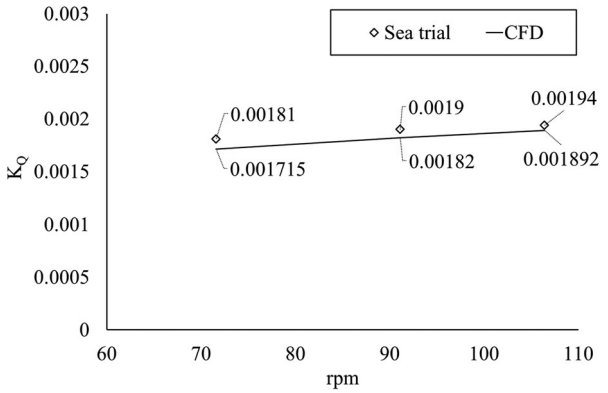

Figure 7. Comparison of torque coefficients between sea trial and CFD.

as shown in Figure 6. The torque coefficient $K_Q$was determined according to Equation (8):

$$K_Q = Q/\rho_{water} n^2 D^5 \tag{8}$$

where Q is the propeller torque, calculated as the surface integral of fluid force in the y-direction times its distance to the propeller centre; D is the diameter of the propeller and n is the shaft revolutions (rotation per second).

Figure 7 compares the sea trial K_Q with that calculated from CFD, where good agreement was achieved. The deviation is less than 5%, which can result from combined errors from RANS, discretisation, uncertainties and statistics (Freitas 2002; Celik et al. 2008; Pena and Huang 2021). This deviation level is deemed to be small enough for the present study, while it is worth noting that the deviation from RANS could be further reduced by using a Detached Eddy Simulation

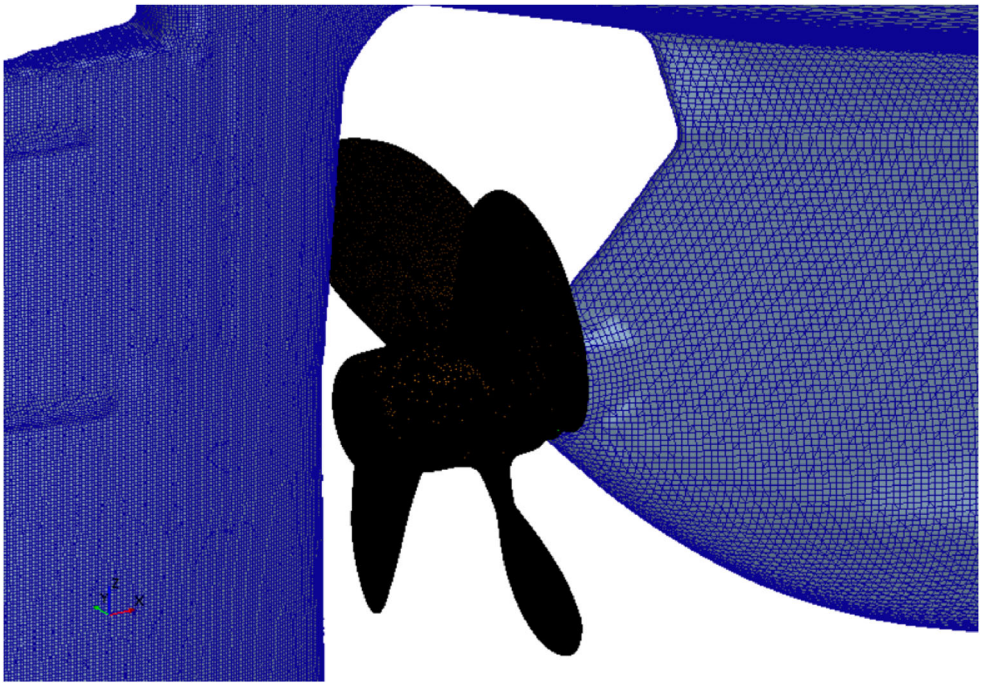

Figure 6. Close-up mesh view around the propeller.

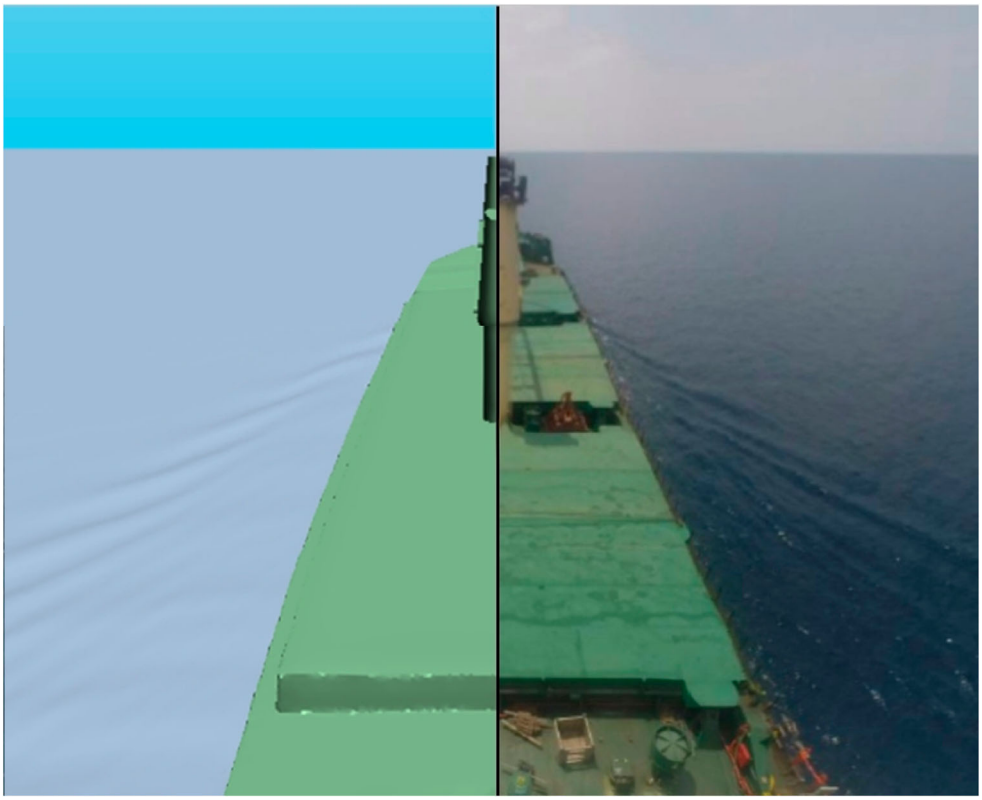

Figure 8. Comparison of ship-generated waves between CFD and photoshoot during the sea trial, rpm = 71.6 (Lloyds Register 2016).

(DES) turbulence modelling method (Pena et al. 2020b). DES however would lead to a much higher computational cost, thus the current study focuses on RANS.

The ship-generated waves were also compared between full-scale CFD and the sea trials, as shown in Figure 8. Despite the sea trials do not have quantified measurements of the free surface elevation, it can be seen from the photo that full-scale CFD can reproduce the vessel-generated wave pattern with high fidelity, demonstrating that the fluid behaviours are correctly retained at the real-ship scale. This allows detailed analyses of localized flow behaviours and fluid-structure interactions, one of the advantages of running the simulation directly in full scale.

2.4 Investigation plan

The above work has built a model that can accurately reproduce a full-scale ship advancing in open water. The validated model is therefore now used as a base case (Case 1), which evolves into 34 other cases investigating different computational setups, as listed in Table 3. The 35 cases use systematically different computational setups. A progressive scale factor of $\sqrt{2}$ is used between the cases, since $\sqrt{2}$ is the standard ratio of varying computational setups for ship-related CFD (ASME 2009; ITTC 2017), which is supposed to detect notable influences. Specifically, Cases 2–4 investigate the overall cell number of the simulation, already presented in Section 2.3; Cases 5–17 ascertain the appropriate cell size for the free surface region and Kelvin wave region, to be reported in Section 3.1; Cases 18–28 determine the thickness of near-hull layer mesh and the expansion ratio of mesh thickness between layers, to be presented in Section 3.2; Cases 29–32 and 33–35 respectively study a suitable timestep size and the orders of spatial and temporal discretisations, as in Section 3.3. Considering these cases integrally, a set of ideal computational setups will be deduced in the end.

3. Study on ideal setups

Following the verification and validation, relevant computational setups are subtly and systematically

Table 3. Summary of the investigated CFD cases.

Case number	Investigated computational setup
1	The base case that is validated against sea trials
2–4	Varying total cell number
5–17	Varying mesh refinements in the free surface region and Kelvin wave region
18–22	Varying the thickness of near hull mesh layer
23–28	Varying the expansion ratio between the layers of the near hull mesh
29–32	Varying the Courant number to determine the suitable timestep size
33–35	Varying order of discretisations, as combinations of: Spatial 1st + Temporal 1st Spatial 1st + Temporal 2nd Spatial 2nd + Temporal 1st Spatial 2nd + Temporal 2nd

varied to derive an ideal approach that can minimize computational costs, whilst maintaining the accuracy. This section investigates the least cell number, the largest timestep size and the least orders of discretisation that are required to accurately model the ship-generated wave, hull boundary layer and corresponding resistance components (pressure and friction). By combining the computationally cheapest but still accurate setups, a collective recommendation is formed for the full-scale ship simulation.

3.1 Ship-generated waves

Accurately modelling ship-generated waves requires an appropriate meshing approach for the free surface in the vertical direction and for the Kelvin pattern in the horizontal direction, which is important for correctly predicting the flow behaviour and ship resistance (especially the pressure component). For this purpose, it is recommended to refine the mesh in the key regions whilst applying relatively coarse meshes in other regions. This treatment helps minimize the computational cost, known as the local mesh refinement, which is especially useful considering the enormous domain dimension of full-scale ship simulations.

Figure 9 demonstrated the mesh refinements recommended by this work, including the dimensions of each refining region. For both the vertical and horizontal directions, three refinement regions are applied to gradually transform the mesh. The gradual mesh scaling is for avoiding a dramatic change of cell sizes between a refined region and its outer region that can cause significant numerical errors and even lead to simulation divergence.

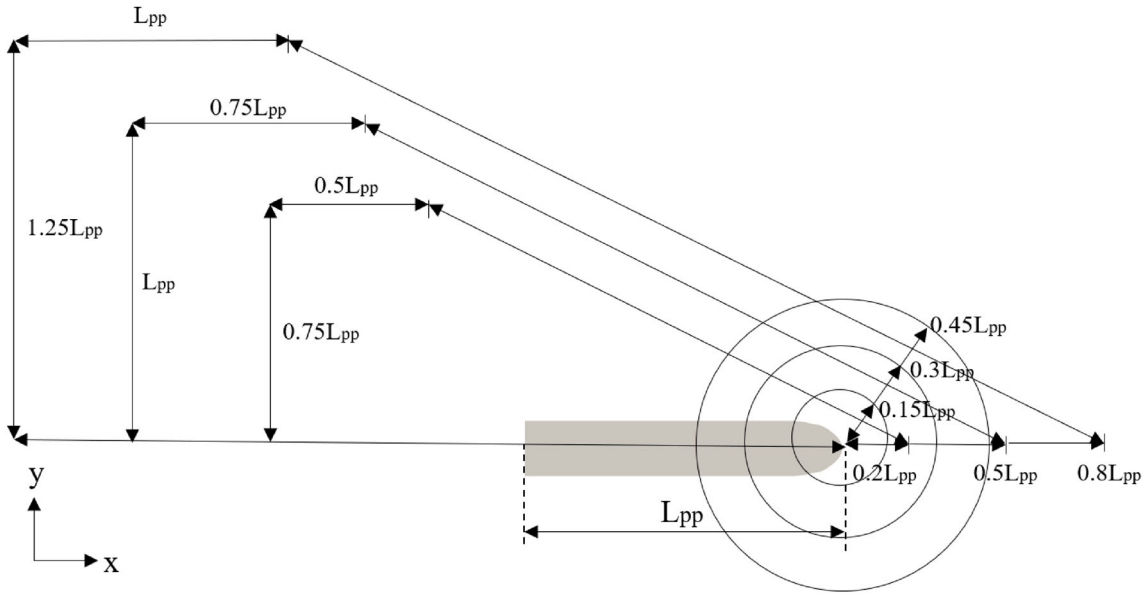

(a) Horizontal regions

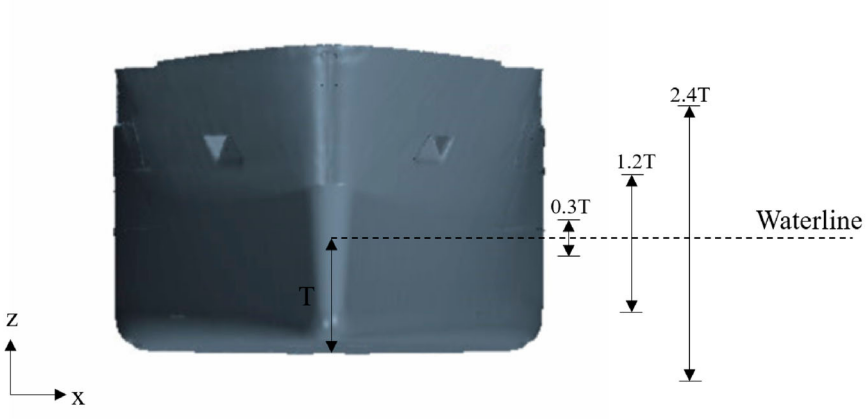

(b) Vertical regions

Figure 9. Mesh refinement regions for modelling ship-generated waves. (a) Horizontal regions; (b) Vertical regions.

Each horizontal-refining region consists of a circle area for bow waves, a triangle of a 20-degree acute angle to cover the Kelvin angle (~19.47 °), as well as a rectangular area for wave radiations accounting for the relative speed between ship and water, presented in Figure 9(a). Each vertical-refining region expands vertically from the waterline to both the upside and downside, as presented in Figure 9(b). The refined mesh is finest in the innermost region, gradually increasing outwards; following this order, the cell sizes in the horizontal regions are donated by ΔX_1, ΔX_2 and ΔX_3, where $\Delta Y = \Delta X$ in each level, and the cell sizes in the vertical regions are donated by ΔZ_1, ΔZ_2 and ΔZ_3. The corresponding overall mesh view can be seen in Figure 3.

To investigate the ideal mesh setups to model the ship-generated waves, the refinement mesh densities for the horizontal and vertical regions were evolved into six extra cases respectively, as listed in Table 4, in which, ΔX and ΔZ are nondimensionalised by ship beam (B) and ship draught (T). The results were analysed using the pressure resistance coefficient (C_P), converting from pressure resistance component (R_P) by $C_P = R_P/0.5\rho_{water}S_w U_{ship}^2$, since this is dominated by changes in the wave.

The changing trend of C_P with different cell sizes in the mesh refinement regions is plotted in Figure 10. It shows the change in the horizontal direction is less sensitive than in the vertical direction. Also, with the mesh density being reduced, the convergence of C_P changes from stable, as in Figure 11(a), to unstable, as in Figure 11(b) where C_P oscillates at the tail. The upper and lower limits of the time-domain oscillation are plotted as error bars in Figure 10. When the mesh becomes sufficiently dense, the oscillating level becomes less than 1% of the magnitude, which is negligible and hardly distinguishable. Therefore, there are no error bars for those cases.

To keep an accurate resistance prediction while minimizing computational costs, the selected cell sizes are $\Delta X_1 = 0.044B$ (Case 7) and $\Delta Z_1 = 0.017T$ (Case 12); these are the suitable mesh densities for C_P, which were tested separately.

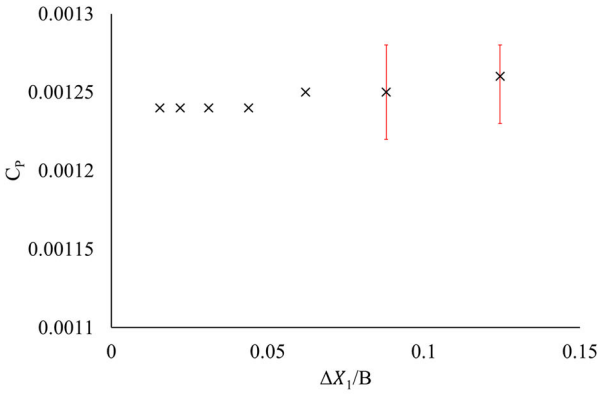

(a) Varying mesh size in horizontal regions

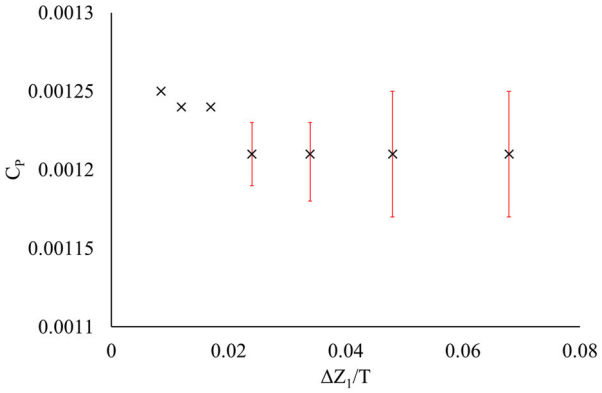

(b) Varying mesh size in vertical regions

Figure 10. Pressure resistance coefficient obtained with different mesh setups in the refinement regions, alongside error bars showing the upper and lower limits of its oscillation along with numerical calculations. (a) Varying mesh size in horizontal regions; (b) Varying mesh size in vertical regions.

Then, an extra test (Case 17) combines both the selected cell sizes from Case 7 and Case 12 to further confirm the accuracy, and the results were similar to the validated case (Case 1). By optimizing the mesh refinements for modelling ship-generated waves, the total cell number of the CFD model was successfully reduced from 15.2 million in Case 1 to 11.7 million in Case 17, while the two cases can get the same accurate results.

Table 4. Mesh setup of the cases studying the modelling of ship-generated waves.

	ΔX_1, ΔY_1	ΔX_2, ΔY_2	ΔX_3, ΔY_3	ΔZ_1	ΔZ_2	ΔZ_3
Case 1 (base)	0.022B	0.044B	0.088B	0.012T	0.048T	0.096T
Case 5	base/$\sqrt{2}$				base	
Case 6	base*$\sqrt{2}$					
Case 7	base*2					
Case 8	base*2$\sqrt{2}$					
Case 9	base*4					
Case 10	base*4$\sqrt{2}$					
Case 11	base				base/$\sqrt{2}$	
Case 12					base*$\sqrt{2}$	
Case 13					base*2	
Case 14					base*2$\sqrt{2}$	
Case 15					base*4	
Case 16					base*4$\sqrt{2}$	
Case 17	0.044B	0.088B	0.176B	0.017T	0.068T	0.136T

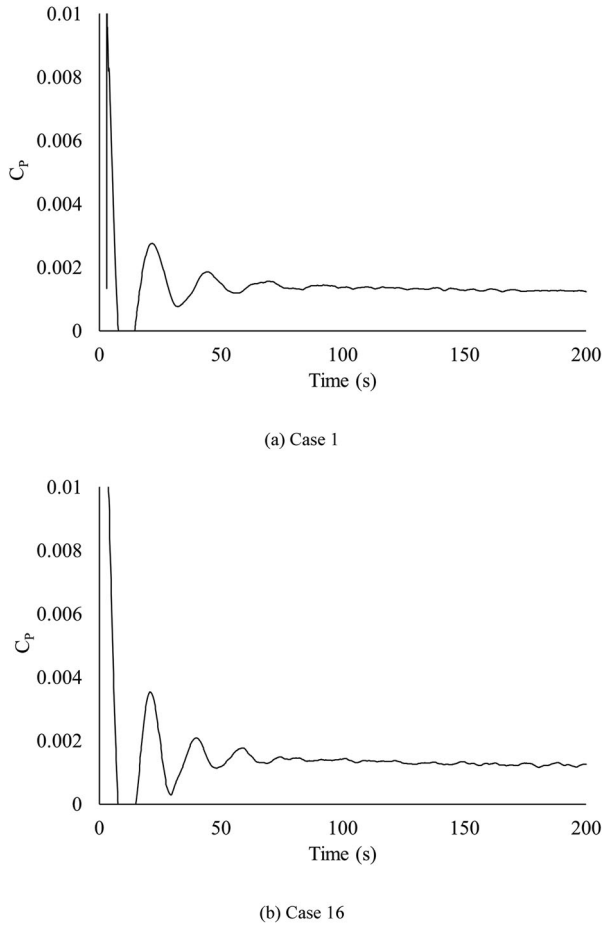

Figure 11. Time series of pressure resistance coefficient; right panel showing an undesired oscillation at the tail. (a) Case 1; (b) Case 16.

3.2 Boundary-layer flow around the ship

The boundary-layer flow around the ship is modelled by mesh layers built upon the hull surface, in which, the layer attaching to the hull is thinnest, and the thickness of each layer gradually increases outwards, so that the thickness of the outmost layer is close to the size of cells outside the mesh layers, as shown in Figure 12. To properly model the boundary layer flow, it is necessary to know (a) the total thickness of the layers (b) how thin the layers should be, and (c) what ratio should the layer thickness increase to. The boundary layer thickness on the majority of the wetted surface of a vessel at 13 knots is measured to be around $\delta = 0.015$ m (Ohta et al. 2008), while the thickness can progressively thicken towards the aft region (Pena et al. 2020a). Therefore, criterion (a), the total thickness of the layer-mesh region, was set at a conservative level of 0.1 m to capture the boundary-layer regions. For criteria (b) and (c), sensitivity analyses are performed to investigate their ideal setups, which is done through varying the thickness of the innermost near-wall layer, h, and the thickness expansion ratio between layers (E).

Table 5. Mesh setup of the cases studying the modelling of hull boundary layer.

	h/δ	$\sim Y^+$	E
Case 17 (base)	0.3	1000	1.2
Case 18	base/$\sqrt{2}$	700	base
Case 19	base*$\sqrt{2}$	1400	
Case 20	base*2	2000	
Case 21	base*2$\sqrt{2}$	3000	
Case 22	base*4	5000	
Case 23	base		1.1
Case 24			1.3
Case 25			1.5
Case 26			1.8
Case 27			2.2
Case 28			3

The test cases are listed in Table 5, combining different sets of layer thickness and expansion ratio for the layer-mesh region; the optimized case from Section 3.1, Case 17, was adopted as the base case here. The results were analysed using the

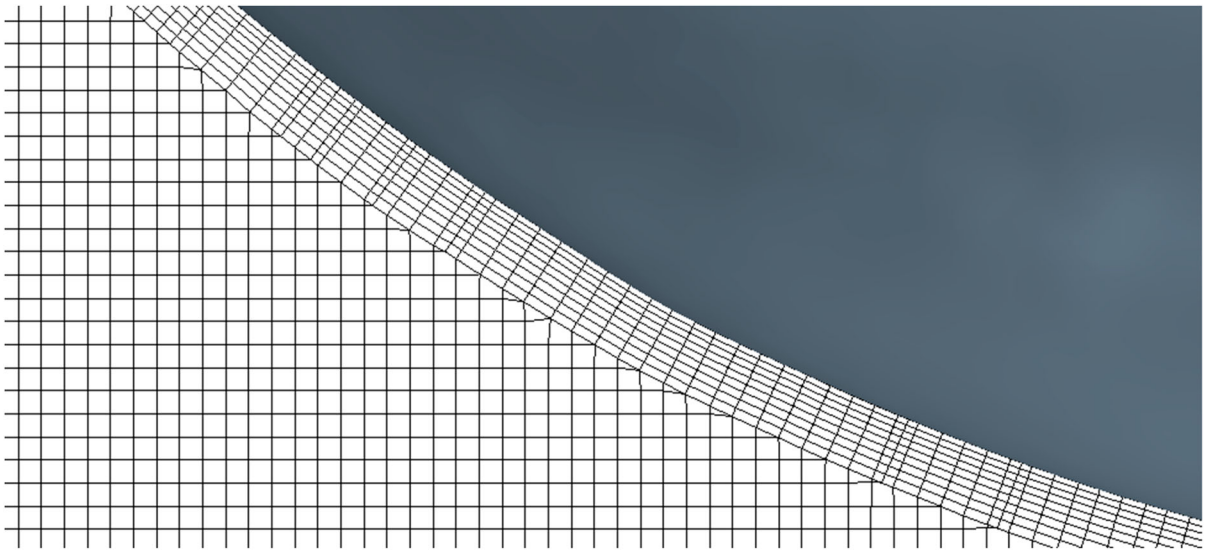

Figure 12. Near-hull mesh setup: mesh layers were built between the hull geometry (upper right) and the regular mesh domain (lower left); dense mesh was applied near the hull surface, which gradually coarsens away from the hull surface.

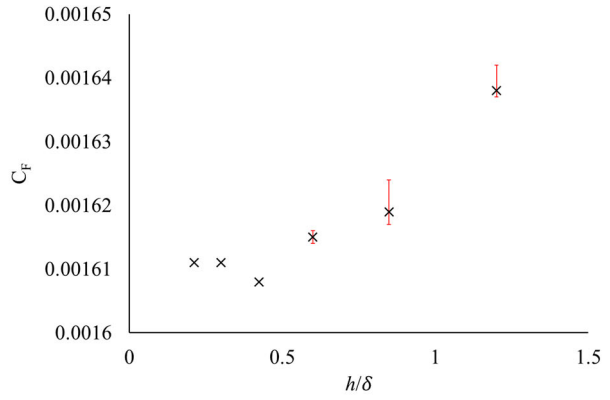

(a) C_F as a function of near-wall cell thickness

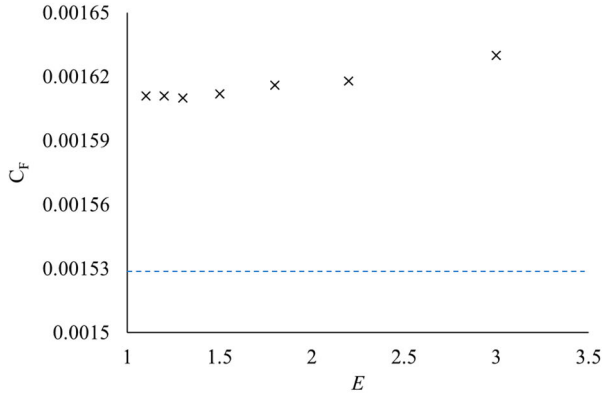

(b) C_F as a function of the expansion ratio for mesh layers

Figure 13. Frictional resistance coefficient obtained with different mesh setups in the boundary layer region, alongside error bars showing the upper and lower limits of its oscillation along with numerical calculations. Dash line shows the corresponding prediction using the ITTC57 method. (a) C_F as a function of near-wall cell thickness; (b) C_F as a function of the expansion ratio for mesh layers.

friction resistance coefficient (C_F), converting from friction resistance component (R_F) by $C_F = R_F/0.5\ \rho_{water} S_w U_{ship^2}$, since this directly reflects the boundary layer effect.

The influences of the layer thickness and expansion ratio on C_F are shown in Figure 13. Figure 13 (a) shows that C_F starts to diverge when $h/\ \delta$ is larger than 0.3. This means that the thickness of the innermost mesh layer cell should be less than 30% of the actual boundary layer thickness. Figure 13(b) shows that E should be no larger than 1.5 to secure the convergence of the solution. On account of these results, the setups in Case 25 are optimal, i.e. $h/\ \delta = 0.3$ and E = 1.5.

To further check the accuracy of the friction prediction, C_F predicted by the widely used ITTC57 empirical equation is also included in Figure 13(b), expressed as Equation (9) (ITTC 2014b). It can be seen that the CFD results are around 5-10% larger than the ITTC57 results. This agrees with the validation for full-scale ship simulations by Niklas and Pruszko (2019) and by Eça and Hoekstra (2008), both reporting their full-scale CFD prediction of C_F is around 5-10% larger than the ITTC57 line. This is also the case for the LR workshop (2016), in which all participants reported that full-scale CFD predicts higher frictional resistance than the ITTC57 line. Thus, the contemporary ITTC formula appears to underestimate C_F in full scale, which is reasonable as the formula is derived based on empirical data in model scale. This suggests an updated version of ITTC equations may be derived when more full-scale measurements and quality CFD data become available, e.g. through a similar

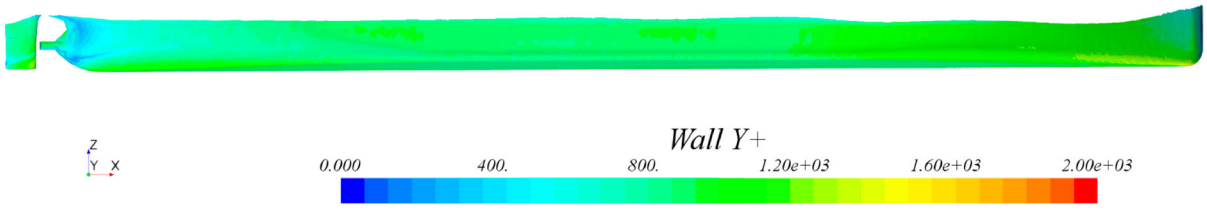

Figure 14. Y^+ value on the hull surface when a reasonable solution can be obtained (Case 17): despite that in model-scale Y^+ is suggested to be $\leq$ 100 for RANS, this proves that in full-scale Y^+ can be around 1000.

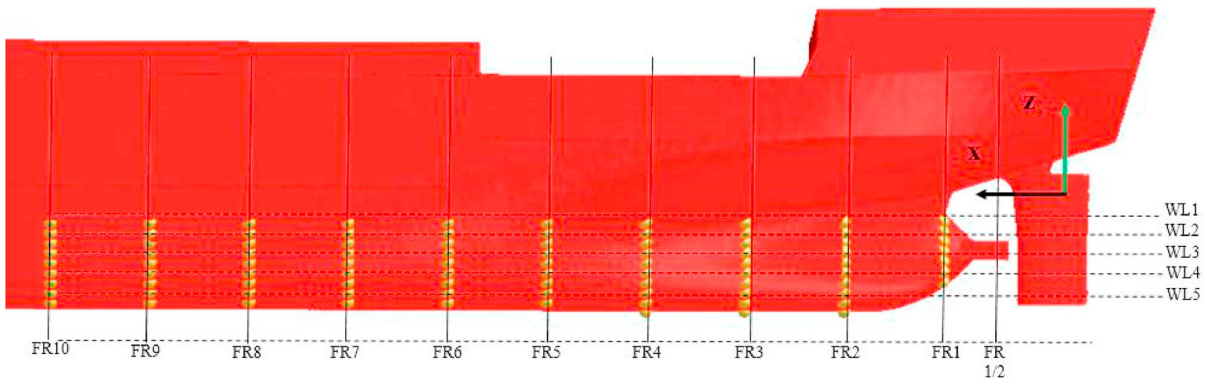

Figure 15. The definition of *Regal*'s frames for boundary layer analysis.

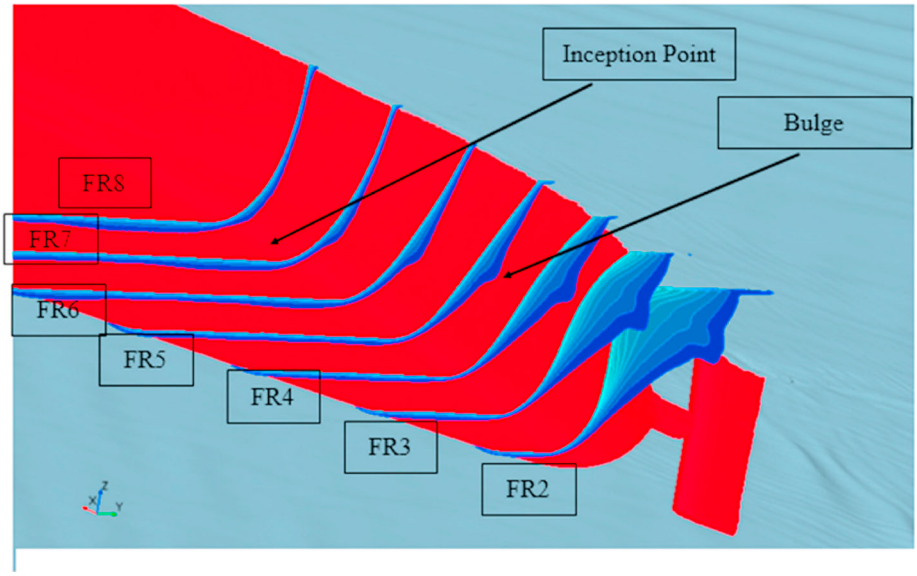

Figure 16. Boundary layer on each frame of the ship.

Table 6. Setup of the cases for studying numerical resolutions, with the rightest column showing the costed computational time using 256 processors.

	$\overline{Co}$	Spatial OD	Temporal OD	Computational time
Case 25 (base)	10	2nd	1st	2 h 7 min
Case 29	base/2	base	base	3 h 30 min
Case 30	base/$\sqrt{2}$			2 h 35 min
Case 31	base*$\sqrt{2}$			1 h 47 min
Case 32	base*2			divergent
Case 33	10	1st	1st	2 h 1 min
Case 34		1st	2nd	1 h 55 min
Case 35		2nd	2nd	1 h 55 min

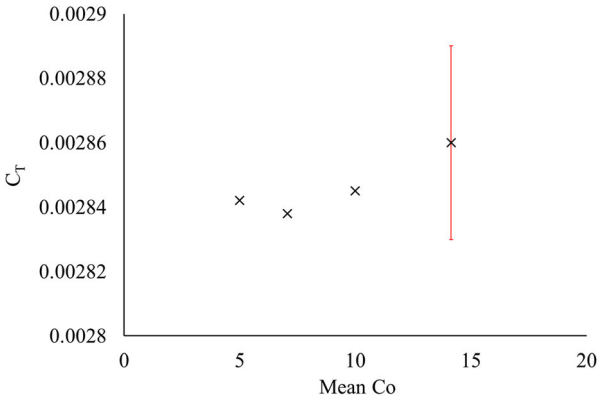

Figure 17. Total resistance coefficients obtained with different timestep sizes, alongside error bars showing the upper and lower limits of its oscillation along with numerical calculations.

procedure as in (Huang et al. 2021a).

$$C_F = 0.075/(\log_{10}Re - 2)^2 \tag{9}$$

The near-wall cell thickness h can be converted into a non-dimensional value Y^+ that is commonly used to guide the construction of the boundary layer mesh in CFD. The expression of Y^+ is taken from (ITTC 2014a) and given as Equation (10) here. Figure 14 presents the Y^+ is around 1000 for $h/\delta = 0.3$, when accurate results were obtained in this work. Whilst the current ITTC guideline suggests Y^+ to be less than 100 for RANS simulations of the same case in model scale (ITTC 2014a), this result shows that it can be unnecessary to use such a low Y^+ value in full scale. Particularly, this signifies a considerable waste of computational resources if following the model-scale standard to build full-scale simulations. This finding corroborates the inference of Peric (2019).

$$Y^+ = \frac{h}{L_{pp}} \times Re\sqrt{0.0375/(\log_{10}Re - 2)^2} \tag{10}$$

More detailed analyses of the boundary layer have also been conducted, in which ten frames (FR) were

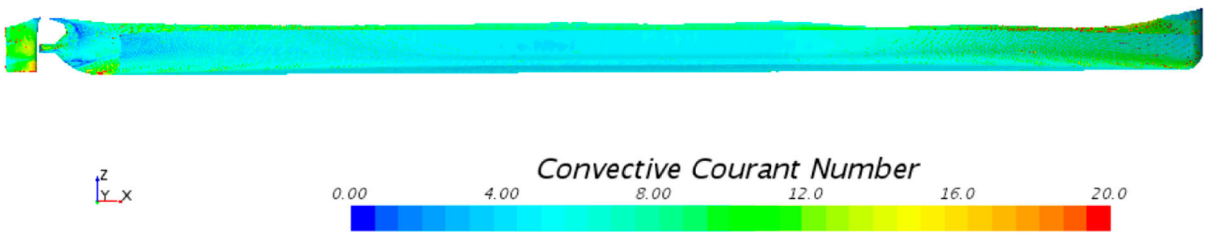

Figure 18. Co value on the hull surface when a reasonable solution can be obtained (Case 25): despite that in model-scale Co is required to be ≤ 1, this proves that in full-scale Co can be around 10.

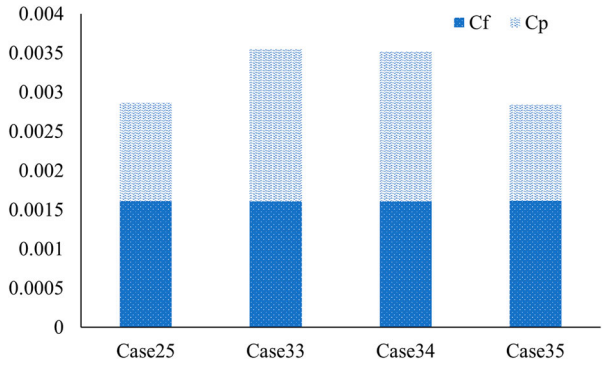

Figure 19. C_P and C_F obtained with different temporal and spatial ODs; the percentages of friction and pressure components are approximated at 44% and 56% for the sensible cases (Cases 25 and 35).

identified on the ship, as shown in Figure 15, and the flow in each FR was investigated. The simulated boundary layers are shown in Figure 16, where the visualized boundary layers were filtered according to the criterion of horizontal velocity equals to or less than $0.99U_{water}$. A thickening boundary layer towards the downstream direction can be seen, and a bulge is formed and grows whilst the boundary layer thickens. Nonetheless, since the sea trial did not provide measurements on the ship's boundary flow details, specific CFD setup for this level of flow details cannot be investigated as part of this work, while a full report on the boundary layer analysis can be found in (Pena et al. 2020a).

3.3 Numerical schemes

There are two types of discretisation in the FVM computation, respectively in space and time. In space, the computational domain is divided into a set of non-overlapping cells, known as a mesh; in time, the temporal dimension is split into a finite number of timesteps. For a single timestep, the solution of the governing equations can be obtained in each cell (e.g. **v**, P, α), and the whole fluid domain can be integrated by the solution obtained for all cells. Then, the fluid domain over a certain time duration is the composition of the fluid domain at each timestep. Following previous sections that investigated different mesh setups, this section studies how to set an appropriate

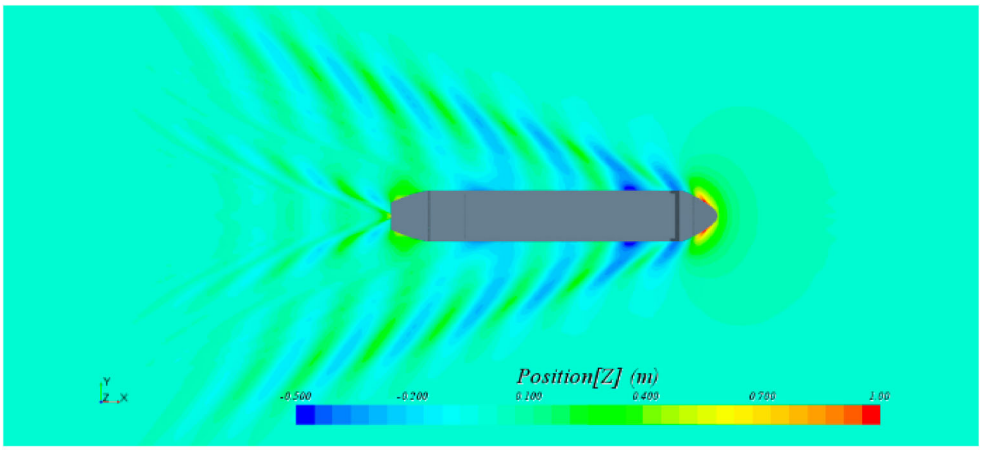

(a) Case 25/35: 2nd spatial OD

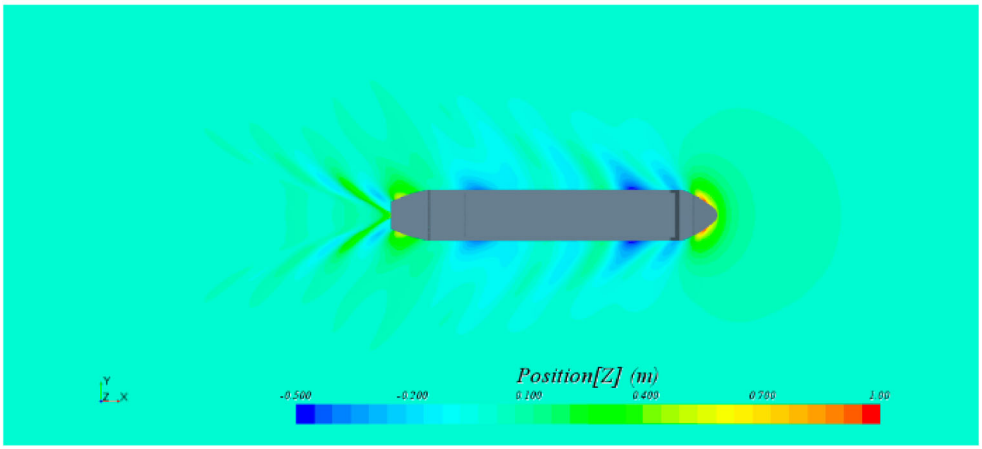

(b) Case 33/34: 1st spatial OD

Figure 20. A comparison showing that 1st order spatial discretisation fails in modelling the ship-generated waves, as in the right panel. (a) Case 25/35: 2nd spatial OD; (b) Case 33/34: 1st spatial OD.

Table 7. Recommended setups for full-scale simulations of a cargo ship in open water.

Ship-generated waves	Layout: Figure 8	Cell size: Case 17 in Table 4
Boundary layer	Layout: Figure 11	Cell size: Case 25 in Table 5
Numerical ODs	Spatial: 2^{nd}	Temporal: 1st/2nd
Computational costs	Cell number: ~11 Million. $\overline{Co} \leq 10$	
	Computational time: ~2 hrs using 256 processors	

timestep size, Δt, and the Order of Discretisation (OD) in spatial and temporal domains. The corresponding test cases are shown in Table 6.

The timestep size is controlled by prescribing the mean value of Courant number as given in Equation (8). Figure 17 shows the influence of the timestep size on the total resistance of the ship, in which the resistance is close to the verified value when $\overline{Co} \leq 10$ and a large change occurred when $\overline{Co}$ was increased to be larger than 10. Similar to the finding on Y+, the threshold value of $\overline{Co}$ in full scale (≤ 10, as shown in Figure 18) is much larger than that in the current model-scale guideline which suggests $\overline{Co}$ to be ≤ 1.

A further investigation was conducted on the OD. For CFD ship simulations, common-used ODs for temporal and spatial discretisations are 1st and 2^{nd} orders; details of the algorithms are given in (Kuzmin 2010). Therefore, there are four tests in this regard by the matrix of 1st and 2nd temporal ODs vs 1st and 2nd spatial ODs. Figure 19 shows that the four sets predict almost identical friction resistance, while 1st spatial OD induced a significant overprediction in pressure resistance (see Case 33 and 34). This means although all four sets of ODs are capable of modelling the hull boundary layer, 1st spatial OD is incapable of modelling ship-generated waves, which is further corroborated by Figure 20. Therefore, it is necessary to apply 2^{nd} spatial OD. For 1st and 2^{nd} temporal OD, they took similar computational time and have no notable difference between their computational results. Therefore, both 1st and 2^{nd} temporal OD are applicable; this finding is in line with the ITTC model-scale recommendation (ITTC 2014a).

4. Conclusions

There are clear benefits from running full-scale CFD simulations to predict ship performance as it can reproduce the ship hydrodynamics at the correct scale, which enables various design activities and avoid uncertainty from conducting model-scale extrapolation procedures. The accuracy of full-scale ship simulations is dictated by computational setups, and the suitable setups differ considerably from those in current model-scale guidelines.

To investigate ideal computational setups for full-scale ship CFD and contribute to its future guidelines, this work first developed a full-scale model for simulating a cargo ship advancing in open water and validated the model against sea trials. Subsequently, a series of simulations were performed to investigate the influences of most important computational setups on the simulation results. These setups include mesh density, mesh transition ratio, mesh local refinements, timestep size, and the orders of discretisations. Their influences are studied on the predictions of ship resistance, ship-generated waves and the ship's boundary layer flow.

An optimized set of setups were obtained that can minimize the computational cost whilst keeping the accuracy, as summarized in Table 7. The present work deduced the computationally cheapest but still accurate mesh density possible, resulting in a total cell number of around 11 million. In addition, it was shown that the most inner layer-mesh thickness around the hull should be less than 30% of the expected boundary layer thickness, while the stretching layers can gradually increase their thickness at a ratio of 1.5. Moreover, it was demonstrated that the 2^{nd} order must be used for spatial discretisation while either the 1st or 2^{nd} order can be used for temporal discretisation. In particular, the results highlight that the suitable Y^+ and timestep sizes for full-scale ship simulations can be approximately ten times those in the current model-scale guideline. Such differences in mesh and timestep selections indicate the importance to develop a separate guideline for full-scale ship CFD. Otherwise, there can exist significant wastes of computational resources, as users might just follow the model-scale guideline to set up full-scale cases.

The present methodology could also be applied to study the full-scale ship CFD for other applications, such as predicting a ship's seakeeping, manoeuvring, and performance in restricted waters. Noting that this work only investigated one hull form, the recommended mesh setup can be adapted to other hull forms, based on the given ratios between mesh densities and ship particulars. However, since the studied ship size is 138 m, for another ship that has a significantly different size, e.g. a small boat, some of the recommendations may need to be derived separately, as such a size difference could cause a scale effect.

In practical engineering design, the recommended full-scale CFD setups are beneficial in terms of helping users set up similar simulations with correct numerics and minimal computational resources, which has been a key element in contemporary developments for the

industry of ships as well as offshore structures (Lloyds Register 2016; Fazeres-Ferradosa et al. 2019, 2020; Terziev et al. 2022). However, noting that the verification and validation in this work were conducted on a global quantity (resistance), the accuracy of the recommended CFD setup in local flow details was not evaluated. Other CFD setups might be needed for ship hydrodynamic applications that rely on local flow details, e.g. cavitation (Lu et al. 2012) and hydroacoustics (Smith and Ventikos 2021). It is expected that future ship operations will include more sensors to obtain local measurements on flow and structural details, which will provide essential data for validating the full-scale CFD of this field as well as inform the optimization of ship performance (Huang et al. 2022).

Disclosure statement

No potential conflict of interest was reported by the author (s).

ORCID

Luofeng Huang http://orcid.org/0000-0002-7096-7677

References

ASME. 2009. Verification & Validation in Computational Fluid Dynamics & Heat Transfer [WWW Document]. URL https://www.asme.org/codes-standards/find-codes-standards/v-v-20-standard-verification-validation-computational-fluid-dynamics-heat-transfer (accessed 2.21.20).

Bakica A, Vladimir N, Gatin I, Jasak H. 2020. CFD simulation of loadings on circular duct in calm water and waves. Ships Offsh Struct. 1–13.

Bhushan S, Xing T, Carrica P, Stern F. 2009. Model-and full-scale URANS simulations of Athena resistance, powering, seakeeping, and 5415 maneuvering. J Ship Res. 53:179–198.

Celik IB, Ghia U, Roache PJ, Freitas CJ, Coleman H, Raad PE, Celik Ì, Freitas C, Coleman HP. 2008. Procedure for estimation and reporting of uncertainty due to discretization in CFD applications. J Fluids Eng.

Cheng C, Xu P-F, Cheng H, Ding Y, Zheng J, Ge T, Sun D, Xu J. 2020. Ensemble learning approach based on stacking for unmanned surface vehicle's dynamics. Ocean Eng. 207:107388.

Eça L, Hoekstra M. 2008. The numerical friction line. J Mar Sci Technol. 13:328–345.

el Moctar O, Shigunov V, Zorn T. 2012. Duisburg Test Case: Post-panamax container ship for benchmarking. Ship Technol Res. 59:50–64.

Fazeres-Ferradosa T, Rosa-Santos P, Taveira-Pinto F, Pavlou D, Gao F-P, Carvalho H, Oliveira-Pinto S. 2020. Preface: advanced research on offshore structures and foundation design: part 2. Proc Inst Civ Eng Marit Eng. 173:96–99. doi:10.1680/jmaen.2020.173.4.96.

Fazeres-Ferradosa T, Rosa-Santos P, Taveira-Pinto F, Vanem E, Carvalho H, Correia J. 2019. Editorial: Advanced research on offshore structures and foundation design: part 1. Proc Inst Civ Eng Marit Eng. 172:118–123. doi:10.1680/jmaen.2019.172.4.118.

Freitas CJ. 2002. The issue of numerical uncertainty. Appl Math Model. 26:237–248. doi:10.1016/S0307-904X(01)00058-0.

Gatin I, Vukčević V, Jasak H, Seo J, Rhee SH. 2018. CFD verification and validation of green sea loads. Ocean Eng. 148:500–515.

Haase M, Davidson G, Binns J, Thomas G, Bose N. 2017. Full-scale resistance prediction in finite waters: A study using computational fluid dynamics simulations, model test experiments and sea trial measurements. Proc Inst Mech Eng M: J Eng Marit Environ. 231:316–328.

Haase M, Zurcher K, Davidson G, Binns JR, Thomas G, Bose N. 2016. Novel CFD-based full-scale resistance prediction for large medium-speed catamarans. Ocean Eng. 111:198–208.

Hirt CW, Nichols BD. 1981. Volume of fluid (VOF) method for the dynamics of free boundaries. J Comput Phys. 39:201–225.

Huang L, Li Y. 2022. Design of the submerged horizontal plate breakwater using a fully coupled hydroelastic approach. Comput-Aided Civ Infrastruct Eng. 37:915–932. doi:10.1111/mice.12784.

Huang L, Li Z, Ryan C, Ringsberg JW, Pena B, Li M, Ding L, Thomas G. 2021a. Ship resistance when operating in floating ice floes: Derivation, validation, and application of an empirical equation. Mar Struct. 79:103057.

Huang L, Pena B, Liu Y, Anderlini E. 2022. Machine learning in sustainable ship design and operation: A review. Ocean Eng. 266.

Huang L, Tavakoli S, Li M, Dolatshah A, Pena B, Ding B, Dashtimanesh A. 2021b. CFD analyses on the water entry process of a freefall lifeboat. Ocean Eng. 232:109115.

Huang L, Tuhkuri J, Igrec B, Li M, Stagonas D, Toffoli A, Cardiff P, Thomas G. 2020. Ship resistance when operating in floating ice floes: A combined CFD&DEM approach. Mar Struct. 74:102817.

ITTC. 2008. 1978 Ittc performance prediction method. Recommended Procedures and Guidelines.

ITTC. 2014a. Guidelines: practical guidelines for ship CFD applications. ITTC Report.

ITTC. 2014b. Example for uncertainty analysis of resistance tests in towing tanks. Recommended Procedures and Guidelines.

ITTC. 2017. Uncertainty analysis in CFD verification and validation methodology and procedures. Recommended Procedures and Guidelines.

Jasak H, Vukčević V, Gatin I, Lalović I. 2019. CFD validation and grid sensitivity studies of full scale ship self propulsion. Int J Nav Archit Ocean Eng. 11:33–43.

Kuzmin D. 2010. A guide to numerical methods for transport equations. University Erlangen-Nuremberg 24.

Liefvendahl M, Fureby C. 2017. Grid requirements for LES of ship hydrodynamics in model and full scale. Ocean Eng. 143:259–268. doi:10.1016/j.oceaneng.2017.07.055.

Lloyd's Register. 2016. Workshop on Ship Scale Hydrodynamic Computer Simulation Proceedings.

Lu NX, Svennberg U, Bark G, Bensow R. 2012. Numerical simulations of the cavitating flow on a marine propeller. in: 8th International Symposium on Cavitation.

McVicar J, Lavroff J, Davis MR, Thomas G. 2018. Fluid–structure interaction simulation of slam-induced bending in large high-speed wave-piercing catamarans. J Fluids Struct. 82:35–58.

Menter F. 1993. Zonal two equation kw turbulence models for aerodynamic flows. in: 23rd Fluid Dynamics, Plasmadynamics, and Lasers Conference. 2906.

Min K-S, Kang S-H. 2010. Study on the form factor and full-scale ship resistance prediction method. J Mar Sci Technol. 15:108–118.
Mucha P. 2017. On Simulation-based Ship Maneuvering Prediction in Deep and Shallow Water (PhD). University of Duisburg-Essen.
Niklas K, Pruszko H. 2019. Full-scale CFD simulations for the determination of ship resistance as a rational, alternative method to towing tank experiments. Ocean Eng. 190:106435.
Nisham A, Terziev M, Tezdogan T, Beard T, Incecik A. 2021. Prediction of the aerodynamic behaviour of a full-scale naval ship in head waves using Detached Eddy Simulation. Ocean Eng. 222:108583.
Ohta S, Shigetomi A, Tasaka Y, Murai Y, Takeda Y, Hinatsu M, Kodama Y. 2008. Boundary layer measurement of a vessel sailing over the sea. in: Proceedings of the 6th International Symposium on Ultrasound Doppler Methods. 139–142.
Paterson EG, Wilson RV, Stern F. 2003. General-purpose parallel unsteady rans ship hydrodynamics code: Cfdshipiowa., IIHR Report 432. Iowa Institute for Hydraulic Research. The University of Iowa, Iowa, USA.
Pena B, Huang L. 2021. A review on the turbulence modelling strategy for ship hydrodynamic simulations. Ocean Eng. 241:110082.
Pena B, Muk-Pavic E, Fitzsimmons P. 2020a. Detailed analysis of the flow within the boundary layer and wake of a full-scale ship. Ocean Eng. 218:108022.
Pena B, Muk-Pavic E, Thomas G, Fitzsimmons P. 2020b. An approach for the accurate investigation of full-scale ship boundary layers and wakes. Ocean Eng. 214:107854.
Peric M. 2019. White paper: full-scale simulation for marine design. Siemens White Pap. 1–14.
Ponkratov D, Zegos C. 2015. Validation of ship scale CFD self-propulsion simulation by the direct comparison with sea trials results. in: Proceedings of the Fourth International Symposium on Marine Propulsors.
Smith TA, Ventikos Y. 2021. Wing-tip vortex dynamics at moderate Reynolds numbers. Phys Fluids. 33:035111.
Smith TA, Ventikos Y. 2022. A hybrid computational aero-acoustic model with application to turbulent flows over foil and bluff bodies. J Sound Vib. 116773.
Terziev M, Tezdogan T, Incecik A. 2019. A geosim analysis of ship resistance decomposition and scale effects with the aid of CFD. Appl Ocean Res. 92:101930.
Terziev M, Tezdogan T, Incecik A. 2021. A numerical assessment of the scale effects of a ship advancing through restricted waters. Ocean Eng. 229:108972.
Terziev M, Tezdogan T, Incecik A. 2022. Scale effects and full-scale ship hydrodynamics: a review. Ocean Eng. 245:110496.
Tezdogan T, Demirel YK, Kellett P, Khorasanchi M, Incecik A, Turan O. 2015. Full-scale unsteady RANS CFD simulations of ship behaviour and performance in head seas due to slow steaming. Ocean Eng. 97:186–206. doi:10.1016/j.oceaneng.2015.01.011.
Tezdogan T, Incecik A, Turan O. 2016. A numerical investigation of the squat and resistance of ships advancing through a canal using CFD. J Mar Sci Technol. 21:86–101.
Versteeg HK, Malalasekera W. 2007. An introduction to computational fluid dynamics: the finite volume method. Pearson Education.